Branched-Chain α-Keto Acid Dehydrogenase Complex from Bovine Kidney: Radial Distribution of Mass Determined from Dark-Field Electron Micrographs†

Marvin L. Hackert,*,‡ Wei-Xin Xu,‡ Robert M. Oliver,‡ Joseph S. Wall,§ James F. Hainfeld,§ Thomas R. Mullinax,‡,∥ and Lester J. Reed‡

Clayton Foundation Biochemical Institute and Department of Chemistry, The University of Texas at Austin, Austin, Texas 78712, and Biology Department, Brookhaven National Laboratory, Upton, New York 11973

Received February 3, 1989; Revised Manuscript Received April 12, 1989

ABSTRACT: Scanning transmission electron microscopy (STEM) was used to determine the radial distribution of mass within the bovine kidney branched-chain α-keto acid dehydrogenase complex (E_1–E_2) and its core enzyme, dihydrolipoamide acyltransferase (E_2). The particle mass of E_2 measured by STEM is $(1.19 \pm 0.02) \times 10^6$. Assuming 24 subunits per E_2 core, this value corresponds to a subunit molecular weight of $(4.96 \pm 0.08) \times 10^4$, which agrees well with the subunit molecular weight estimated by sodium dodecyl sulfate–polyacrylamide gel electrophoresis of 5.2×10^4 (Pettit et al., 1978) and that deduced from the gene sequence, 46 518 (Griffin et al., 1988). Thus, the STEM data reaffirms the 24-subunit model for this E_2. Previous studies indicated that the E_2 subunits contain an extended, outer lipoyl-bearing domain connected by a trypsin-sensitive segment to a compact, inner catalytic domain. The assemblage of 24 inner domains comprises a cubelike inner core. The quantity and spatial distribution of mass determined from STEM images for the E_2 inner core are consistent with this model. The lipoyl-bearing domains are shown to occupy a zone defined by radii of 80–130 Å over which the lipoyl moiety may range. This zone overlaps the positions of the 24 branched-chain α-keto acid dehydrogenase (E_1) molecules, which apparently are located on the edges of the cubelike inner core.

α-Keto acid dehydrogenase complexes from prokaryotic and eukaryotic sources are composed of multiple copies of three enzymes: an α-keto acid dehydrogenase (E_1),[1] a dihydrolipoamide acyltransferase (E_2), and the flavoprotein dihydrolipoamide dehydrogenase (E_3). The oligomeric E_2 component comprises a symmetrical core around which are arranged multiple copies of E_1 and E_3 (Reed, 1974; Oliver & Reed, 1982). Results of electron microscopic studies (Reed & Oliver, 1968), X-ray crystallographic studies (DeRosier et al., 1971; Fuller et al., 1979), and sedimentation equilibrium molecular weight determinations (Pettit et al., 1973; Eley et al., 1972) demonstrated that the E_2 components of the *Escherichia coli* pyruvate and α-ketoglutarate dehydrogenase complexes each consist of 24 apparently identical subunits arranged with 432 molecular symmetry in a cubelike particle.

Analysis of the *E. coli* dihydrolipoamide acetyltransferase (E_2) by controlled proteolysis with trypsin revealed that these E_2 subunits contain two major domains—an extended, outer lipoyl-bearing domain and a compact, inner catalytic and subunit-binding domain (Bleile et al., 1979). This unique architectural feature is exhibited by all dihydrolipoamide acyltransferases. The assemblage of compact, catalytic, and subunit-binding domains constitutes the "inner core" of E_2. Removal of the bristlelike lipoyl domains from the *E. coli* dihydrolipoamide acetyltransferase does not alter the cubelike appearance or dimensions of the inner core as observed by negative-stain electron microscopy. These findings have been confirmed and extended by molecular genetics (Stephens et al., 1983; Guest et al., 1984) and ^{1}H NMR spectroscopy (Perham et al., 1981; Radford et al., 1987).

The appearance of the E_2 component of the mammalian branched-chain α-keto acid dehydrogenase complex (BCKADC) as observed by negative-stain electron microscopy is very similar to the appearance of the E_2 components of the *E. coli* pyruvate and α-ketoglutarate dehydrogenase complexes, indicating that the former E_2 also consists of 24 subunits (Pettit et al., 1978; Oliver & Reed, 1982). The molecular mass of the subunit of E_2 from BCKADC is 46 518 Da, determined from the gene sequence (Griffin et al., 1988). Compared to the value of 1 110 000 Da for the whole E_2 component, as determined by sedimentation equilibrium, a 24-mer stoichiometry of E_2 is supported (Griffin et al., 1988). Limited proteolysis with trypsin of the E_2 from BCKADC releases the outer lipoyl-bearing domains from the inner core without changing the core morphology (Hu et al., 1986; Chuang et al., 1985). The molecular mass values for inner catalytic and subunit-binding domain and lipoyl-bearing domain are 27 013 and 19 523 Da, respectively, on the basis of the gene sequence. During purification of BCKADC, E_3 dissociates from the complex (Pettit et al., 1978). Therefore, the highly purified complex consists of E_1 and E_2. It is estimated that about 24 molecules of E_1 are attached to the E_2 core (Reed et al., 1985). E_1 consists of two distinct subunits, $E_{1\alpha}$ and $E_{1\beta}$, with apparent M_rs of about 46 000 and 35 000, respectively (Pettit et al., 1978). The former value compares favorably with a calculated M_r of 45 709 for $E_{1\alpha}$ from rat liver based on the deduced amino acid sequence from the cloned cDNA (Zhang et al., 1987).

† This work was supported in part by Grants GM 30105 (M.L.H.) and GM 06590 (L.J.R.) from the National Institutes of Health, U.S. Public Health Service.

* Address correspondence to this author.
‡ University of Texas at Austin.
§ Brookhaven National Laboratory.
∥ Present address: Du Pont NEN, Boston, MA 02118.

[1] Abbreviations: STEM, scanning transmission electron microscopy; E_2, dihydrolipoamide acyltransferase; E_1, branched-chain α-keto acid dehydrogenase; BCKADC, branched-chain α-keto acid dehydrogenase complex; SDS–PAGE, sodium dodecyl sulfate–polyacrylamide gel electrophoresis; APM_r, average projected mass; RAM, radially accumulated mass; M, shell mass; M_r, molecular mass.

0006-2960/89/0428-6816$01.50/0

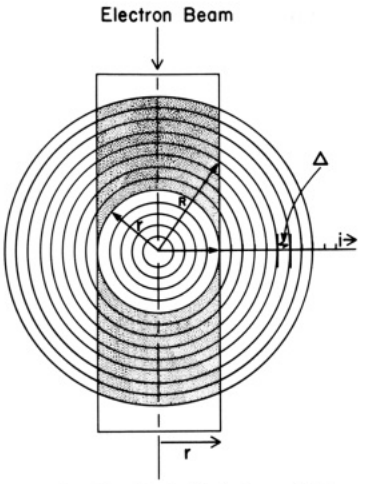

FIGURE 1: Cross section (vertical slice) through the cylindrical and spherical constructs that define the geometric relationships used to compute shell mass values, M_i. (Δ) Spherical shell thickness and cylindrical radius increment; (r) projected (cylindrical) radius; (R) shell radius.

To gain further knowledge of the structure of BCKADC and its E_2 core, images of these proteins observed by scanning transmission electron microscopy (STEM) were analyzed. We present a method for the computation of the three-dimensional, average radial mass distribution of multienzyme complexes from two-dimensional radial mass analysis of STEM images from a population of such particles in which individual particles are presented in random orientations with respect to the scanning electron beam. We have computed the radial mass distributions for the E_2 component of BCKADC from bovine kidney and for a complex that contained E_2 and E_1. The radial mass distribution data are consistent with structural models of E_2 and E_1–E_2 proposed from negative-stain electron microscopic and physicochemical data.

Experimental Procedures

Electron Microscopy and Image Processing. Digital STEM images were recorded at the Brookhaven Biotechnology Resource microscope (Mosesson et al., 1982) and processed by use of the interactive computer-graphics display system previously described (Steven et al., 1984; Hainfeld et al., 1982). The image-processing software allows the user to individually center a set of concentric circles on the image of each of the randomly oriented particles within the population analyzed. The mass estimate associated with a circle of chosen radius, r, corresponds to the projected mass from a cylindrical construct of radius r that traverses the specimen in the direction of the electron beam (see Figure 1). Mass measurements at a series of selected radii that differ by a constant increment (Δ) (usually 10 or 20 Å), are calculated. Repetition of this process on each of a population of particles, where the particles are randomly oriented with respect to the scanning electron beam, yields a set of mass vs radius measurements that are averaged for each radius (r). These average projected mass values (APM_r) depict the projected mass distribution in two dimensions for the population of particles as a function of radius from its center. When the radius of the cylindrical construct equals or exceeds the maximum radial dimension of the particle, APM_r is a measure of the total mass of the particle. Particles of tobacco mosaic virus were included in each sample to provide a mass calibration standard for each set of observations.

Computation of Shell Mass Values. The average radial distribution of mass in three dimensions (average shell mass values, M_i) would be more informative as to architectural features of the particle and can be calculated from the APM_r observations. The same series of radii that defined the set of cylindrical geometric constructs also defines a set of spherical geometric constructs or concentric shells of uniform thickness (Δ) (Figure 1). Because of the geometric relationships extant when the particles are examined, the APM_r value at a selected radius (r) less than the maximum radial dimension of the particle exceeds the mass of that portion of the particle's structure which is contained in the spherical construct defined by that radius. This difference is a measure of mass positioned outside the spherical construct but within the cylindrical construct. Those portions of the cylindrical construct that encompass such mass are structured of cylindrical segments from concentric shells of radii R larger than the construct defining radius r (shaded regions, Figure 1). The average mass contribution from a given shell segment, i, to the APM_r value at a selected radius r will be proportional to the mass, M_i, positioned in the ith shell and to a geometrical coefficient F_i, the fraction of the volume of the ith shell contained in the two cylindrical segments of it that lie within the cylindrical construct. Thus, the APM_r at any selected radius may be expressed by

$$APM_r = F_1M_1 + F_2M_2 + \ldots F_iM_i + \ldots F_nM_n$$

where the subscripts 1–n designate the shells of the spherical construct. The values of the geometrical coefficients, F_j, are dependent on the choice of radius (r); thus, F_j values must be computed for each APM_r measurement. For instance, for the APM_r where the radius r corresponds to the ith shell, all geometrical coefficients F_j for $j \leq i$ are equal to 1, while all F_j for $j > i$ are less than 1.0.

By use of the general expression for APM_r, a set of n simultaneous equations is written for the set of APM_r vs selected radius observations from the population of particles. Solution of these equations yields values for mass contained in the consecutive shells of the spherical construct. This set of shell mass values constitutes the average radial distribution of mass in the structure of the particle. The mass distribution profile of the particle may be graphically presented by plotting M_i vs r, or the data may be used to compute a radial mass density profile.

Another presentation useful in the study of large, oligomeric particles is the profile of radially accumulated mass (RAM). RAM_r values are computed by summing all M_i's contained within the spherical construct to a selected radius, r.

$$RAM_r = \sum_{i=1}^{n} M_i$$

Purification and Resolution of E_1–E_2 Complex. The BCKADC (i.e., E_1–E_2 complex) was purified to near homogeneity from bovine kidney mitochondria as described (Pettit et al., 1978). The E_1–E_2 complex was resolved into E_1 and E_2 by gel filtration in the presence of 1 M NaCl as described by Cook et al. (1985), except that Sephacryl S-300 was used and 1 mM benzamidine was added to the buffer.

Preparation of Protein Samples for STEM. Protein samples were cross-linked with glutaraldehyde essentially as described by CaJacob et al. (1985) for cross-linking the *E. coli* pyruvate dehydrogenase complex. In brief, 1–1.5 mg of protein/mL in 10 mM potassium phosphate buffer (pH 7.0) and 1 mM EDTA was incubated with 0.25 wt % glutaraldehyde for 15 min at 25 °C. Sodium borohydride, 2 mol/mol of glutaraldehyde, dissolved in 0.3 M phosphate buffer (pH 8.0) was added to reduce the aldimine groups and

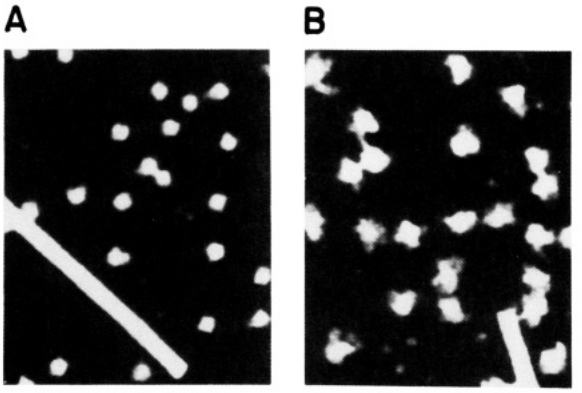

FIGURE 2: STEM dark-field micrographs of E_2 (A) and E_1–E_2 complex (B). In these presentations mass in the unstained particles appears in gray to white shades against the black background. The rodlike structure is tobacco mosaic virus, which served as a mass standard. (Magnification is $\sim 1.39 \times 10^5\times$.)

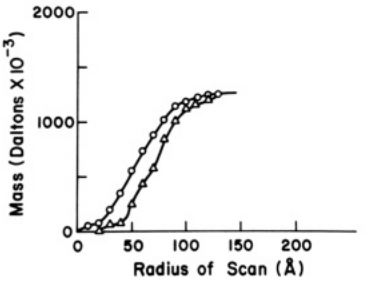

FIGURE 3: Average detected mass APM_r vs radius, r, for E_2 (O). The results are averages of measurements on 87 particles as the radius, r, was increased in increments of 10 Å. (Δ) Radially accumulated mass RAM_r vs radius, r, computed from the APM_r observations on E_2.

thereby stabilize the glutaraldehyde cross-links. After 20 min at 4 °C, 8 molar equiv of sodium pyruvate was added to scavenge the excess glutaraldehyde. The mixture was subjected to gel filtration on a Sephadex G-25 column equilibrated with 20 mM piperazine-*N*,*N*′-bis(2-ethanesulfonate) buffer (pH 7.0), 1 mM benzamidine, 1 mM phenylmethanesulfonyl fluoride, 1 mM EDTA, and 0.01 mM (benzyloxycarbonyl)-phenylalanylalanine diazomethyl ketone, a thiol-protease inhibitor (Watanabe et al., 1979). The effectiveness of cross-linking was confirmed by SDS–PAGE (Laemmli, 1970). When completely cross-linked, no protein bands penetrated the gel. CaJacob et al. (1985) reported that the glutaraldehyde cross-links contributed about 2.7% to the total mass of *E. coli* pyruvate dehydrogenase complex. On the basis of experiments with $Na^{14}CN$, which adds to the aldimine group to form an aminonitrile (Hansen et al., 1974; Bower & Zalkin, 1982), we estimated that the glutaraldehyde cross-links contributed about 2% of the total mass of the protein samples.

Preparation of STEM Specimens. Specimens for STEM examination were adsorbed on carbon films and freeze-dried as described (Mosesson et al., 1982).

Results and Discussion

Radial Distributions of Mass in E_2 and in E_1–E_2 Complex. Micrographs typical of those analyzed in this study are shown in Figure 2. The contrast, while insufficient to display structural details of the particles, was adequate to select individual, well-isolated images for processing; thus, the effect of extraneous contaminants or possible overlap of images are minimized. A population of 372 selected E_2 particles was used to obtain an average M_r of E_2 of $(1.19 \pm 0.02) \times 10^6$. This value compares favorably with a value of 1.12×10^6 calculated

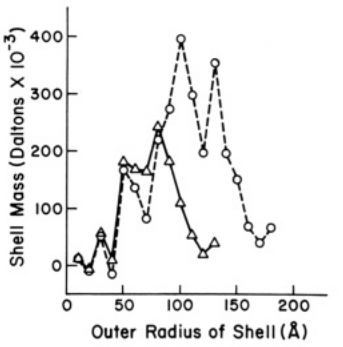

FIGURE 4: Average radial mass distributions in E_2 (Δ) and in the E_1–E_2 complex (O).

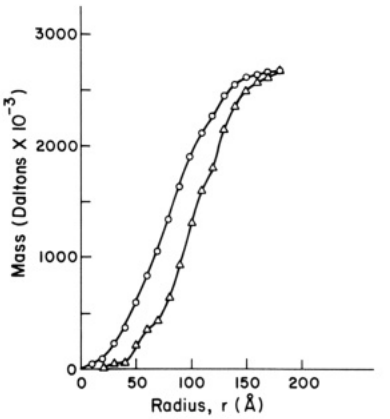

FIGURE 5: Average projected mass (APM_r) vs radius, r, for the E_1–E_2 complex (O). The results are averages of measurements on 87 particles as the radius, r, was increased in increments of 10 Å. (Δ) Radially accumulated mass (RAM_r) vs radius, r, computed from the APM_r observations on the E_1–E_2 complex.

from 24 subunits, each of molecular mass of 46 518 Da (Griffin et al., 1988).

Images from a population of 87 E_2 particles were selected for radial mass analysis. The APM_r data are plotted vs radius, r, in Figure 3. The slope of the curve (Δ) approaches zero at a radius of 130 Å, the apparent outer radial limit of mass of the E_2 structure. At that limit APM_r, the average M_r of the population of particles, is $(1.23 \pm 0.02) \times 10^6$. The shell mass values computed from these observations are plotted vs outer radius of the shell in Figure 4 to graphically illustrate the radial distribution of mass in the E_2. Evidently the center of the particle is practically void of mass to a radius of 20 or 30 Å. The major portion of mass in the structure is located between radii 40 and 90 Å, but significant mass extends to the outer limit of 120 or 130 Å. The RAM_r vs radius, r, plot is also shown in Figure 3. Comparison of the APM_r and RAM_r data indicates the relative magnitude of mass contained within the cylindrical and spherical constructs respectively at the selected radius, r. The slope of the RAM_r curve over each incremental change of radius (Δ) is proportional to the mass resident in the shell defined by that increment. Inflections formed by these incremental slopes may indicate the radial position of significant structural features; such features may not be easily discerned in the presentation of Figure 4.

A second population of 87 particles of the E_1–E_2 complex was selected for analysis. The APM_r vs radius, r, data are plotted in Figure 5. The apparent outer radial limit of mass of the E_1–E_2 complex is 180 Å, and the average M_r of the population is $(2.68 \pm 0.12) \times 10^6$. Shell mass and RAM values computed from these observations are plotted in Figures 4 and 5, respectively. Comparison of the shell mass values from the E_1–E_2 complex with those from E_2 suggests the inner

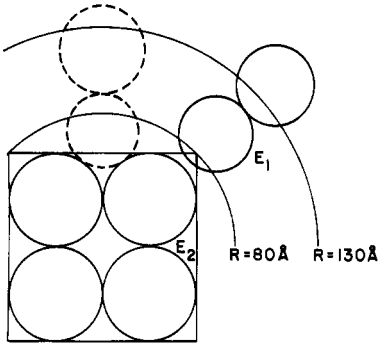

FIGURE 6: Projection along the fourfold symmetry axis of the model of E_2 inner core. In this view, four of the eight trimers of subunit-binding domains are superimposed to form a "tetrad" of mass about the center. The diameter of each trimer is 57 Å. The edges of a cube (edge length 114 Å) that encloses the inner core model are projected as a square. The projection of the intersphere of the enclosing cube is shown at radius 80 Å. The projection of the spherical construct at radius 130 Å marks the outer limit of the zone occupied by the lipoyl-bearing domain. The projection of one of the 24 positions occupied by a molecule of E_1 and aligned according to the mass distribution given in Figure 8 is depicted on the edge of the cube as a solid line, whereas the closer-in position occupied by E_1 if it were bound in a face is represented by a dashed line.

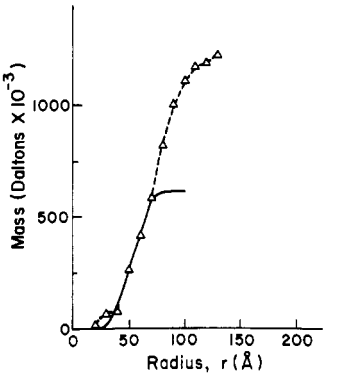

FIGURE 7: Radially accumulated mass (RAM_r) vs radius, r, computed from the APM_r observations on E_2. Solid line (—) RAM_r vs radius, r, computed for the model of the inner core structure of E_2.

radial extent of E_1 mass in the structure is 80 Å, some 40–50 Å inside the outer radial limit of mass of E_2.

Radial Distribution of Mass of the Inner Core of E_2. Electron microscopic and physicochemical data indicate that E_2 from BCKADC consists of 24 apparently identical subunits (46 518 Da) arranged into a cubelike structure with molecular mass of 1.12×10^6 Da (Griffin et al., 1988). Limited proteolysis of E_2 with trypsin releases the bristlelike lipoyl domains from the inner core. The molecular mass of the subunit of the inner core is 27 013 Da as determined from gene sequence (Griffin et al., 1988). Thus, the molecular mass of the inner core is about 648 000 Da.

The simplest model depicting the morphology of the cubelike inner core is constructed by placing a sphere at each of the eight vertices of a cube. Each sphere represents a trimer of catalytic and subunit-binding domains corresponding to a mass of ~81 000 Da. At a normal packing density for protein (0.83 Da/Å^3), the diameter of each sphere is calculated to be 57 Å, and the edge dimension of a cube that encloses the structure is 114 Å. The interradius (defined as the radius of a sphere that touches all edges of a polyhedron) of the cube that encloses the inner core model is approximately 80 Å (see Figure 6). Measurements on a gallery of negative-stain images of the E_2 inner core indicate the edge dimension of the enclosing cube is ~110 Å (Pettit et al., 1978; Oliver and Reed, unpublished data). The RAM_r vs radius, r, curve calculated for the distribution of mass in this model of the inner core (Figure 7) is in good agreement with the RAM curve at radii <80 Å obtained from the STEM observations from intact E_2. The coincidence of this negative stain image-based model dimension with the inflections of the STEM-based RAM curves at radii 70–80 Å from both intact E_2 and the E_2 inner core suggests the inflections mark the proximate radial position of the trypsin-sensitive "hinge" that connects the two principal domains of the E_2 subunit and the outer radial limit of mass of the inner core structure. For the model, the estimated mass of 648 000 Da for the inner core structure is contained within the spherical construct of a radius equal to the interradius of the structure-enclosing cube, 80 Å. The RAM_r vs radius, r, curves indicate that quantity of mass is enclosed by spherical constructs which are of radii <80 Å for both E_2 and E_1–E_2 specimens. Thus, the STEM observations fully support the E_2 inner core model previously advanced. Apparently, in the structure of the E_1–E_2 complex only mass of the catalytic and subunit-binding domain of E_2 is resident within the spherical construct of radius ~80 Å.

Radial Distribution of Mass of the Lipoyl-Bearing Domain of E_2. The outer, lipoyl-bearing domains are connected to the inner, catalytic and subunit-binding domains of E_2 by segments that are rich in proline and alanine residues. These interdomain linker segments (hinge regions) are thought to provide flexibility to the lipoyl-bearing domains, facilitating active-site coupling within the α-keto acid dehydrogenase complexes (Bleile et al., 1979; Perham et al., 1981; Radford et al., 1987). The frictional ratios (f/f_0) of lipoyl-bearing domains isolated from *E. coli* and mammalian dihydrolipoamide acyltransferases were found to be 1.8 and 1.9, respectively (Bleile et al., 1979, 1981). These values indicate that the lipoyl-bearing domains possess an extended or swollen structure. The lipoyl domains in the *E. coli* dihydrolipoamide acyltransferase have the appearance of a "fuzz" around the cubelike inner core (Bleile et al., 1979). In view of these observations and the apparent mobility of lipoyl-bearing domains in several dihydrolipoamide acyltransferases demonstrated by ^{1}H NMR spectroscopy (Perham et al., 1981; Perham & Roberts, 1981), it has not been possible to specify positions and/or ranges of lipoyl moieties in the α-keto acid dehydrogenase complexes. However, the radial distribution of mass of E_2 provides insight as to the positions of the lipoyl-bearing domains in the BCKADC structure and to the radial limits within which the lipoyl moiety might range. Because of the postulated positions and mass of the inner core, mass discerned at radial positions >80 Å in the distribution of E_2 (Figure 4) is considered mass primarily of the lipoyl-bearing domains. The spherical shell defined by radii of 80 and 130 Å is a structural zone in the complex within which the lipoyl moieties may be mobile. This conclusion is in accord with concepts previously proposed of the functional organization of α-keto acid dehydrogenase complexes (Oliver & Reed, 1982).

Radial Distribution of Mass in E_1. Subtraction of shell mass values for E_2 (Figure 4) from the comparable shell mass values for the E_1–E_2 complex yields the radial mass distribution of the E_1 contained in the specimen examined, assuming the M_i values for E_2 remain unchanged upon binding E_1. The average M_r of the population of 237 particles examined, (2.66 ± 0.06) $\times 10^6$, indicates that an average of ~18 E_1 molecules was present in the E_1–E_2 complexes. A subset of 87 such particles was used for radial mass analysis; thus, the distribution resulted from measurement on ~1566 E_1 molecules. The magnitudes of shell mass values plotted in Figure 8A are interpreted as mass resident in each shell from 18 E_1 molecules.

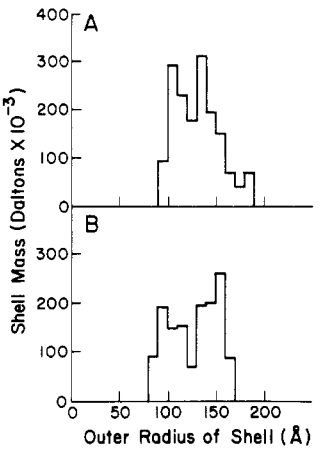

FIGURE 8: (A) Radial distribution of the mass of E_1 in the E_1–E_2 complex. (B) Computed radial distribution of the mass of 18 E_1 molecular models positioned in the structural model (solid lines) of the E_1–E_2 complex depicted in Figure 6.

E_1 is comprised of two subunits, $E_{1\alpha}$ ($M_r \sim 46\,000$) and $E_{1\beta}$ ($M_r \sim 35\,000$) (Pettit et al., 1978). A simple model for this molecule encloses the mass in a sphere ~57 Å in diameter. Since the STEM radial mass extends over a range of ~100 Å, such a model is inadequate. An alternate model encloses each subunit, $E_{1\alpha}$ and $E_{1\beta}$, in spheres of ~47 Å and dimension of ~90 Å. The radial distribution of mass expected for such a bilobular particle can be computed as shown in Figure 8B. The well-defined inflections of the mass curves for the E_1–E_2 specimen (Figure 5) in the region of radii 110–130 Å impose a relatively low value for the mass contained in a shell of radii 120–130 Å (Figure 8A). This suggests, subject to the assumption that the average mass distribution of E_2 changes little upon binding E_1 and the difference curves are meaningful, that the inflections may be indicative of the position of the nexus of the subunits, $E_{1\alpha}$ to $E_{1\beta}$, in the complex. Details of the morphology of E_1 have not been characterized by negative-stain electron microscopy nor has the binding order, E_2–$E_{1\beta}$–$E_{1\alpha}$, suggested by the model been ascertained. Therefore, the significance of the mass curve inflections at radii 110–130 Å is not established. However, if such a particle is placed along the radius of a spherical construct such that the local minimum observed at 120–130 Å aligns with that minimum computed for the model of the $E_{1\alpha}$–$E_{1\beta}$ particle, the result is as illustrated the solid circles shown in Figure 6.

The mass curve inflections at radii 70–80 Å appear to mark the outer radial limit of the inner core structure and the inner radial limit of mass of the E_1 in the complex structure as well. This observation supports a general model for the E_1–E_2 subcomplex previously proposed (Oliver & Reed, 1982) that positioned multiple molecules of component E_1 along the edges of the cubelike inner core as graphically illustrated by Figure 6, where the computed position of a single molecule of E_1 is shown by the solid line. In contrast, if the molecules of E_1 were positioned on the faces of the inner core (dashed lines), two effects should have been observed: (a) the spherical construct of radii ~80 Å, the intersphere of the cubelike core, should have contained more mass than the previously estimated mass of the inner core and (b) the magnitude of RAM curve values from the E_1–E_2 complex would have exceeded comparable values from E_2 at some radius <80 Å. Neither effect was observed. The STEM result, as interpreted, fully supports the model previously proposed for the quaternary organization of BCKADC and, by analogy, the class of α-keto acid dehydrogenase complex systems that are organized by cubelike inner core structures.

Summary

The analysis of dark-field STEM images of a population of randomly oriented particles can provide valuable information about the total mass and radial dimensions of complex particles (Lamvik, 1978; Wall, 1978; Engel, 1983; Steven et al., 1984). While these parameters are basic to any structural model considered, the unique design of the particle is not revealed directly by STEM analysis. Given a particular APM_r vs radius, r, result, a variety of structural models may be considered that could potentially satisfy the observed data. However, when used in conjunction with pertinent information from other sources on structural models, STEM data can be represented in a variety of useful ways and such analysis proves to be a valuable adjunct to the methods heretofore employed in the development of structural and functional models of complex, oligomeric particles.

Frey and co-workers (Yang et al., 1985, 1986) employed STEM and radial mass measurements to examine the pyruvate dehydrogenase complex of *E. coli*. Using the observed, two-dimensional radial mass values, they plotted APM_r ratios of E_1–E_2 and E_2–E_3 subcomplexes to E_2 to reveal the locations of the E_1 and E_3 components. The results they obtained for the radial position of E_1 in the pyruvate dehydrogenase complex are very similar to those reported here for the BCKADC. We have extended this type of analysis by converting the observed, two-dimensional APM_r values into computed, three-dimensional RAM_r values. The result is increased sensitivity, such that not only the radial positions of the particles but also the radial mass distributions of the particles are revealed along with insight concerning subunit and domain structure.

We have employed these techniques to examine structural models of the E_2 core and E_1–E_2 particles from BCKADC. The results provide direct support for a model of E_2 consisting of a hollow center of ~30 Å, an inner core from 40 to 80 Å, and an outer domain that occupies a structural zone from 80 to 130 Å. The data from the E_1–E_2 complex, subject to the assumptions described earlier, indicate that the E_1 particle penetrates the outer regions of the extended lipoyl-bearing domain of E_2 and extends ~50 Å beyond. The data also suggest that E_1 particles possess two morphological domains and occupy binding sites near the edge of the cubelike inner core of E_2. These results support earlier models based on other, indirect, methods. The favorable comparison of the mass distributions obtained directly and indirectly from these studies demonstrates the usefulness of the STEM data and radial reconstruction analysis.

References

Bleile, D. M., Munk, P., Oliver, R. M., & Reed, L. J. (1979) *Proc. Natl. Acad. Sci. U.S.A. 76*, 4385–4389.

Bleile, D. M., Hackert, M. L., Pettit, F. H., & Reed, L. J. (1981) *J. Biol. Chem. 256*, 514–519.

Bower, S., & Zalkin, H. (1982) *Arch. Biochem. Biophys. 219*, 121–127.

CaJacob, C. A., Frey, P. A., Hainfeld, J. F., Wall, J. S., & Yang, H. (1985) *Biochemistry 24*, 2425–2431.

Chuang, D. T., Hu, C.-W. C., Ku, L. S., Markovitz, P. J., & Cox, R. P. (1985) *J. Biol. Chem. 260*, 13779–13786.

Cook, K. G., Bradford, A. P., & Yeaman, S. J. (1985) *Biochem. J. 225*, 731–735.

DeRosier, D. J., & Oliver, R. M. (1971) *Cold Spring Harbor Symp. Quant. Biol. 36*, 199–203.

DeRosier, D. J., Oliver, R. M., & Reed, L. J. (1971) *Proc. Natl. Acad. Sci. U.S.A. 68*, 1135–1137.

Eley, M. H., Namihira, G., Hamilton, L., Munk, P., & Reed, L. J. (1972) *Achiv. Biochem. Biophys. 152*, 655–669.
Engel, A. (1983) *Micron 13*, 425–436.
Fuller, C. C., Reed, L. J., Oliver, R. M., & Hackert, M. L. (1979) *Biochem. Biophys. Res. Commun. 90*, 431–438.
Griffin, T. A., Lau, K. S., & Chuang, D. T. (1988) *J. Biol. Chem. 263*, 14008–14014.
Guest, J. R., Darlison, M. G., Spencer, M. E., & Stephens, P. E. (1984) *Biochem. Soc. Trans. 12*, 220–223.
Hainfeld, J. F., Wall, J. S., & Desmond, E. J. (1982) *Ultramicroscopy 8*, 263–270.
Hansen, B. A., Lane, R. S., & Dekker, E. E. (1974) *J. Biol. Chem. 249*, 4891–4896.
Hu, C.-W. C., Griffin, T. A., Lau, K. S., Cox, R. P., & Chuang, D. T. (1986) *J. Biol. Chem. 261*, 343–349.
Laemmli, U. K. (1970) *Nature 227*, 680–685.
Lamvik, M. K. (1978) *J. Mol. Biol. 122*, 55–68.
Mosesson, M. W., Hainfeld, J., Haschemeyer, R. H., & Wall, J. (1982) *J. Mol. Biol. 153*, 695–718.
Oliver, R. M., & Reed, L. J. (1982) in *Electron Microscopy of Proteins* (Harris, J. R., Ed.) Vol. 2, pp 1–48, Academic Press, London.
Perham, R. N., & Roberts, G. C. K. (1981) *Biochem. J. 199*, 733–740.
Perham, R. N., Duckworth, H. W., & Roberts, G. C. K. (1981) *Nature 292*, 474–477.
Pettit, F. H., Hamilton, L., Munk, P., Namihira, G., Eley, M. H., Willms, C. R., & Reed, L. J. (1973) *J. Biol. Chem. 248*, 5282–5290.
Pettit, F. H., Yeaman, S. J., & Reed, L. J. (1978) *Proc. Natl. Acad. Sci. U.S.A. 75*, 4881–4885.
Radford, S. E., Laue, E. D., Perham, R. N., Miles, J. S., & Guest, J. R. (1987) *Biochem. J. 247*, 641–649.
Reed, L. J. (1974) *Acc. Chem. Res. 7*, 40–46.
Reed, L. J., & Oliver, R. M. (1968) *Brookhaven Symp. Biol. 21*, 397–412.
Reed, L. J., Damuni, Z., & Merryfield, M. L. (1985) *Curr. Top. Cell. Regul. 27*, 41–49.
Stephens, P. E., Darlison, M. G., Lewis, H. M., & Guest, J. R. (1983) *Eur. J. Biochem. 133*, 481–489.
Steven, A. C., Hainfeld, J. F., Trus, B. L., Steinert, P. M., & Wall, J. S. (1984) *Proc. Natl. Acad. Sci. U.S.A. 81*, 6363–6367.
Wall, J. (1978) in *Introduction to Analytical Electron Microscopy* (Hren, J. J., Goldstein, J. I., & Joy, D. C., Eds.) pp 333–342, Plenum, New York.
Watanabe, H., Green, G. D. J., & Shaw, E. (1979) *Biochem. Biophys. Res. Commun. 89*, 1354–1360.
Yang, H., Hainfeld, J. F., Wall, J. S., & Frey, P. A. (1985) *J. Biol. Chem. 260*, 16049–16051.
Yang, H., Frey, P. A., Hainfeld, J. F., & Wall, J. S. (1986) *Biophys. J. 49*, 56–58.
Zhang, B., Kuntz, M. J., Goodwin, G. W., Harris, R. A., & Crabb, D. W. (1987) *J. Biol. Chem. 262*, 15220–15224.

Carbonyl Sulfide Inhibition of CO Dehydrogenase from *Rhodospirillum rubrum*†

Michael R. Hyman,‡ Scott A. Ensign,§ Daniel J. Arp,‡ and Paul W. Ludden*,§

Department of Biochemistry, University of California, Riverside, California 92521, and Department of Biochemistry, College of Agricultural and Life Sciences, University of Wisconsin—Madison, Madison, Wisconsin 53706

Received February 27, 1989; Revised Manuscript Received May 9, 1989

ABSTRACT: Carbonyl sulfide (COS) has been investigated as a rapid-equilibrium inhibitor of CO oxidation by the CO dehydrogenase purified from *Rhodospirillum rubrum*. The kinetic evidence suggests that the inhibition by COS is largely competitive versus CO (K_i = 2.3 μM) and uncompetitive versus methylviologen as electron acceptor (K_i = 15.8 μM). The data are compatible with a ping-pong mechanism for CO oxidation and COS inhibition. Unlike the substrate CO, COS does not reduce the iron–sulfur centers of dye-oxidized CO dehydrogenase and thus is not an alternative substrate for the enzyme. However, like CO, COS is capable of protecting CO dehydrogenase from slow-binding inhibition by cyanide. A true binding constant (K_D) of 2.2 μM for COS has been derived on the basis of the saturable nature of COS protection against cyanide inhibition. The ability of CO, CO_2, COS, and related CO/CO_2 analogues to reverse cyanide inhibition of CO dehydrogenase is also demonstrated. The kinetic results are interpreted in terms of two binding sites for CO on CO dehydrogenase from *R. rubrum*.

Carbon monoxide is oxidized by at least four different classes of enzyme. These are (1) ammonia- and methane-oxidizing monooxygenases found in autotrophic nitrifying bacteria (Tsang & Suzuki, 1982) and methanotrophic bacteria (Colby et al., 1977), respectively; (2) the CO oxidases that are O_2 insensitive, contain molybdenum, Fe-S clusters, and FAD, and are found in aerobic carboxydotrophic bacteria (Meyer, 1985); (3) the CO dehydrogenases that are O_2 labile and multimeric, contain nickel, zinc, and Fe-S clusters, and are found in strictly anaerobic acetogenic and methanogenic bacteria (Drake et al., 1980; Grahame & Stadtman, 1987); and (4) the CO dehydrogenase from *Rhodospirillum rubrum*, which is O_2 labile, monomeric, and contains Fe-S clusters, 1 mol of nickel/mol of enzyme, and substoichiometric amounts of zinc (Bonam et al., 1984, 1988; Ensign et al., 1989a).

Despite superficial similarities, the two classes of nickel-containing CO dehydrogenases are sufficiently different to warrant separate classification. The physiological role of the

† This research was supported by the College of Agricultural and Life Sciences at the University of Wisconsin—Madison and by Grant DE-FG02-87ER13691 to P.W.L. from the U.S. Department of Energy. S.A.E. was supported by Training Grant GM07215 from the National Institutes of Health, and M.R.H. was supported by Grant DE-FG03-84ER13257 to D.J.A. from the U.S. Department of Energy during this study.

* Address correspondence to this author.
‡ University of California.
§ University of Wisconsin—Madison.

0006-2960/89/0428-6821$01.50/0